Engineering Failure Analysis

A water droplet erosion-induced fatigue crack propagation and failure in X20Cr13 martensitic stainless-steel turbines working at low pressure

--Manuscript Draft--

Manuscript Number:	EFA-D-22-00546R2
Article Type:	Research Paper
Keywords:	erosion-fatigue, failure analysis, turbine, x20cr13 martensitic stainless steel, water droplet erosion
Corresponding Author:	SASIKUMAR CHANDRABALAN, Ph.D. Maulana Azad National Institute of Technology Bhopal, Madhya Pradesh INDIA
First Author:	Sarim Khan Mohd, M.Tech.
Order of Authors:	Sarim Khan Mohd, M.Tech.
	SASIKUMAR CHANDRABALAN, Ph.D.
Abstract:	A low-pressure steam turbine blade failed at a thermal power plant reported in this paper. Few blades were damaged on the exhaust side, and the cracks originated on the trailing edge and spread toward the leading edge of blade. In the crack initiation point, shallow corrosion pits were evident, however, turbine vibrations were found to be actuating crack initiation and propagation. Due to numerous pits observed on blades surface, there were vibrations. A pressure drop on the exhaust side of the steam turbine caused condensation and water droplets impinging on the blades caused severe erosion. Upon contact with the condensed water droplets, the chromium carbide precipitates in the martensitic matrix converted into chrome oxides, and impingement of high velocity steam erodes these oxides, causing a rough surface with honeycombed texture. As a result of the roughened blade surfaces, fatigue cracks form at potentially weaker areas and subsequently the final fracture.
Suggested Reviewers:	Modi Om Prakash, Ph.D. Scientist CSIR-AMPRI (ex), AMPRI: Advanced Materials and Processes Research Institute CSIR omprakashmodi56@gmail.com Expert failure analysis
	Mondal D P, Ph.D. Cheif Scientist, AMPRI: Advanced Materials and Processes Research Institute CSIR mondaldp@ampri.res.in Expert in this field
	Mukhopadhyay N K, Ph.D. Professor, IIT BHU: Indian Institute of Technology BHU Varanasi mukho.met@iitbhu.ac.in expert in this field
Response to Reviewers:	

COVERING LETTER

Date: 15.03.2022

To

The Editor-in-Chief,
Engineering Failure Analysis

Dear Editor-in-Chief,

Sub: Submission of article for publication in the **"Engineering Failure Analysis" reg**.

Warm Greetings!

We would like to submit a manuscript paper titled" **A water droplet erosion-induced fatigue crack propagation and failure in X20Cr13 martensitic stainless-steel turbines working at low pressure** " for possible consideration and publication in your journal as a regular paper.

The paper submitted is our original experimental work carried out at the Department of Materials and Metallurgical Engineering, MANIT Bhopal, India. In this work we report a case study on the failure of turbine blade in thermal power station.

"I write on behalf of myself and all co-authors to confirm that the results reported in the manuscript are original and neither the entire work, nor any of its parts have been previously published. The authors confirm that the article has not been submitted to peer review, nor has been accepted for publishing in another journal. The author(s) confirms that the research in their work is original, and that all the data given in the article are real and authentic. If necessary, the article can be recalled, and errors corrected."

I hereby assure that the contents of this article are original and are not copied from any of the existing artifacts / papers/ documents etc.,. It has neither been published elsewhere in any language fully or partly, nor under review for publication anywhere.

I further affirm that other author(s) of this paper have seen, validated, verified for its authenticity and agreed to the submitted version of the manuscript and inclusion of his / her / their name(s) as Co-author(s).

Name and Address of the Corresponding Author:
Dr C Sasikumar, Assistant Professor
Department of Materials and Metallurgical Engineering, MANIT Bhopal,
Madhya Pradesh-462003, India.
Mobile Number:8989005394, E-mail id.:csasimv@gmail.com,
Alternate email id: c.sasikumar.manit@nic.in

Signature of the Corresponding Author

Novelty statement

- This article reports turbine blade failures caused by a combination of corrosion, erosion, and vibration followed by fatigue crack growth and failure. Interestingly, although deep pits can be seen on the leading edges of the blades, the fatigue crack propagates from the trailing edge.

Conflict of Interest Disclosure Form

I/we certify the following statements

The authors have no relevant financial or non-financial interests to disclose.
The authors have no conflicts of interest to declare that are relevant to the content of this article.
All authors certify that they have no affiliations with or involvement in any organization or entity with any financial interest or non-financial interest in the subject matter or materials discussed in this manuscript.
The authors have no financial or proprietary interests in any material discussed in this article.

Corresponding author

Highlights

- Turbine blade failures caused by mixed factors, including corrosion, erosion, and turbine vibrations, followed by fatigue crack growth and failure is reported.
- In this study, we identified the transformation of chromium carbide precipitates in the martensitic matrix into chrome oxides during steam condensation.
- Our study examines how steam impingement eroding these chromium oxides changes the surface roughness of turbine blades and how that affects the turbine vibrations.
- The exhaust side of the steam turbine was subjected to a pressure drop, which caused pitting corrosion, corrosion, and surface roughness on the blades.
- . Although deep pits are created on the leading edges of the blades, it's interesting to note that the fatigue crack propagates from the trailing edge.

List of figures

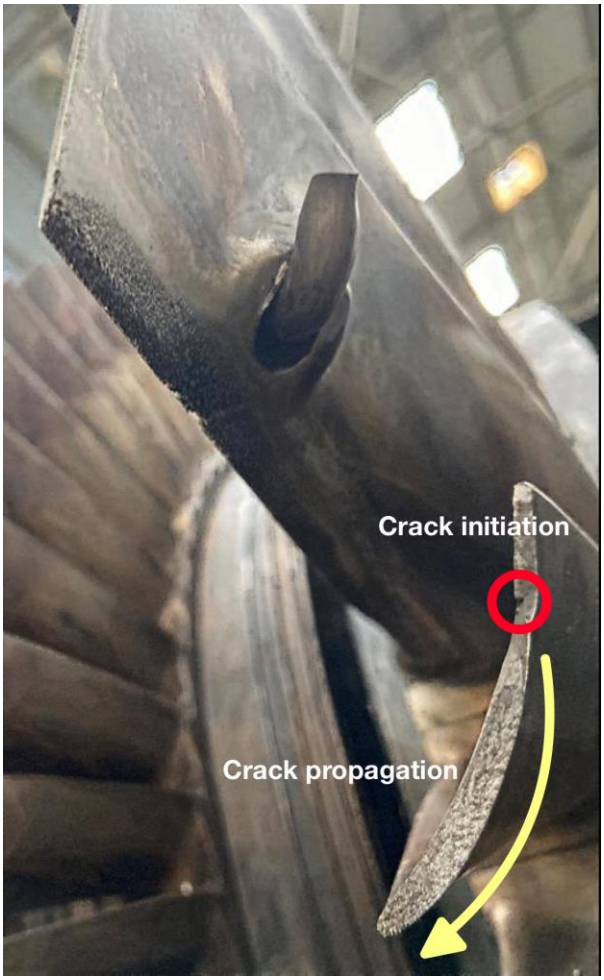

Fig. 1. In the photograph, a fracture is visible about 100 mm from the root of the turbine blade on the exhaust side of the stream turbine.

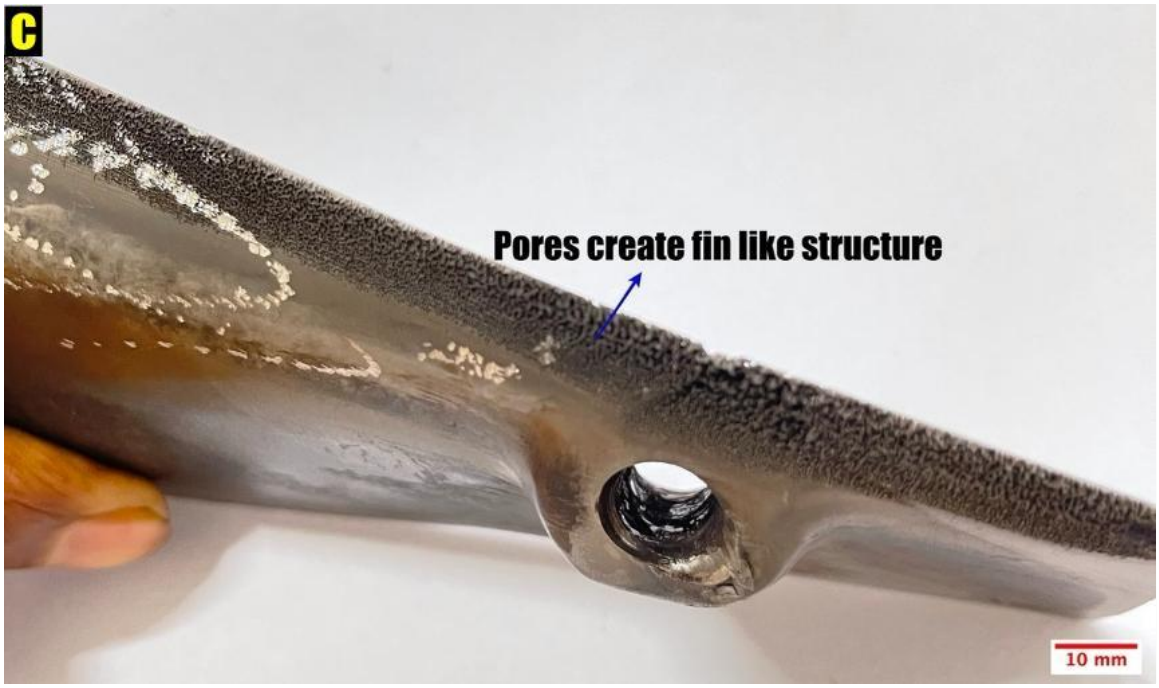

Fig. 2(a, b, c). The leading edges of turbine blades located on the exhaust side show several pits/grooves, an apparent fin-like texture.

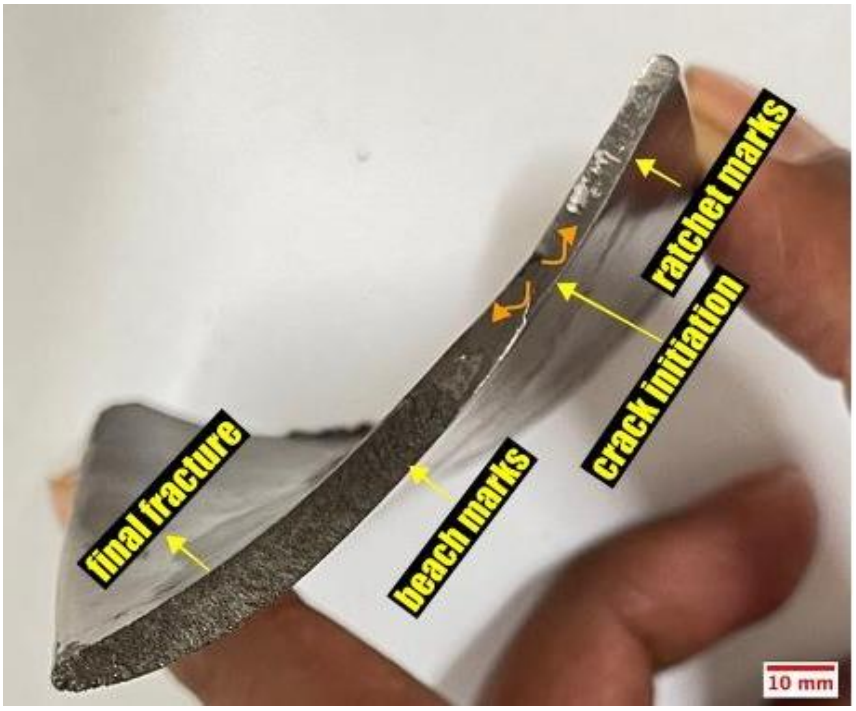

Fig. 3. Fracture surfaces shown in (a) concave and (b) convex perspectives, and (c) cross sections demonstrating crack initiation point, crack propagation region with beach marks and the final fast fracture region.

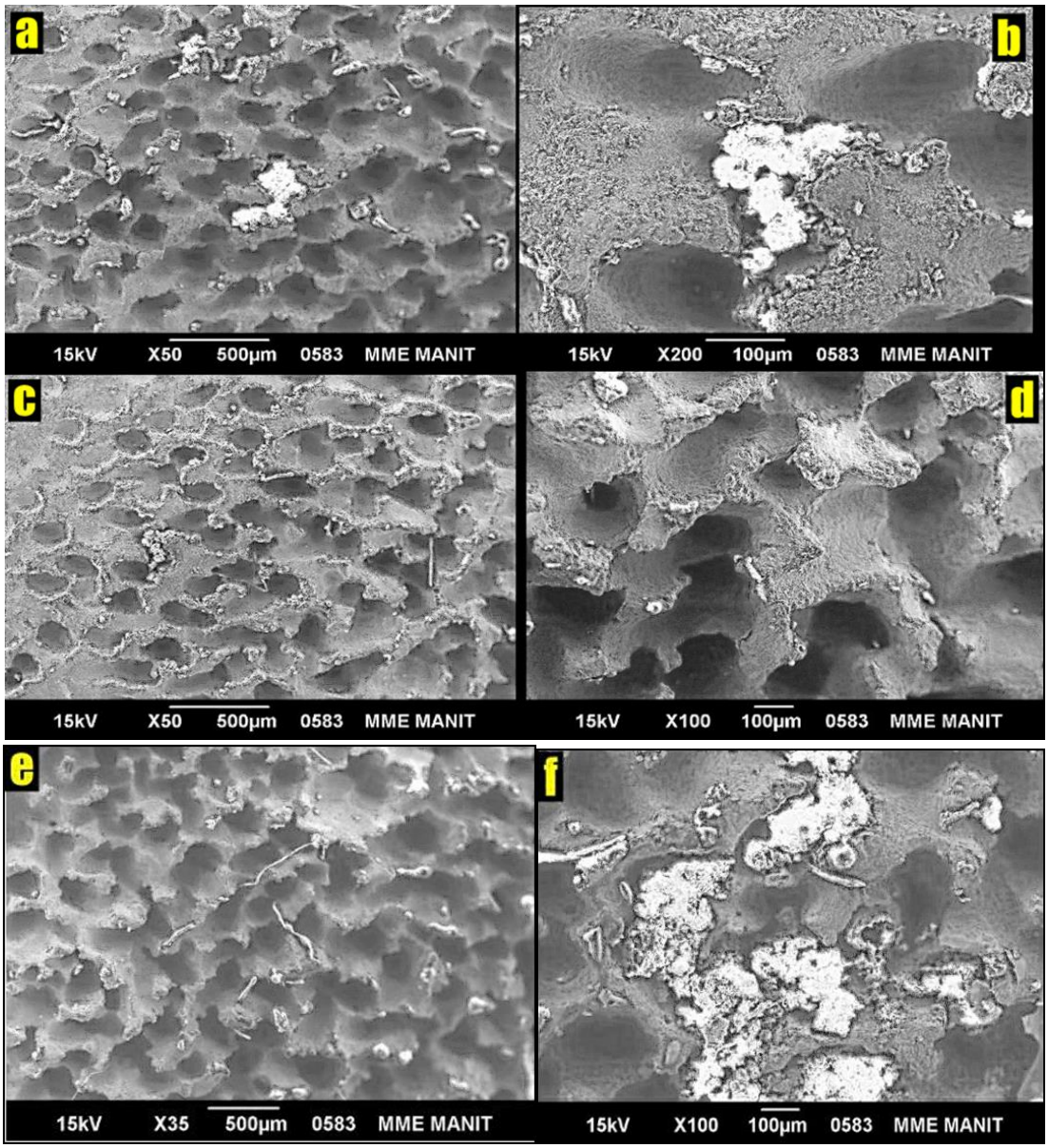
a
15kV X50 500µm 0583 MME MANIT
b
15kV X200 100µm 0583 MME MANIT
c
15kV X50 500µm 0583 MME MANIT
d
15kV X100 100µm 0583 MME MANIT
e
15kV X35 500µm 0583 MME MANIT
f
15kV X100 100µm 0583 MME MANIT

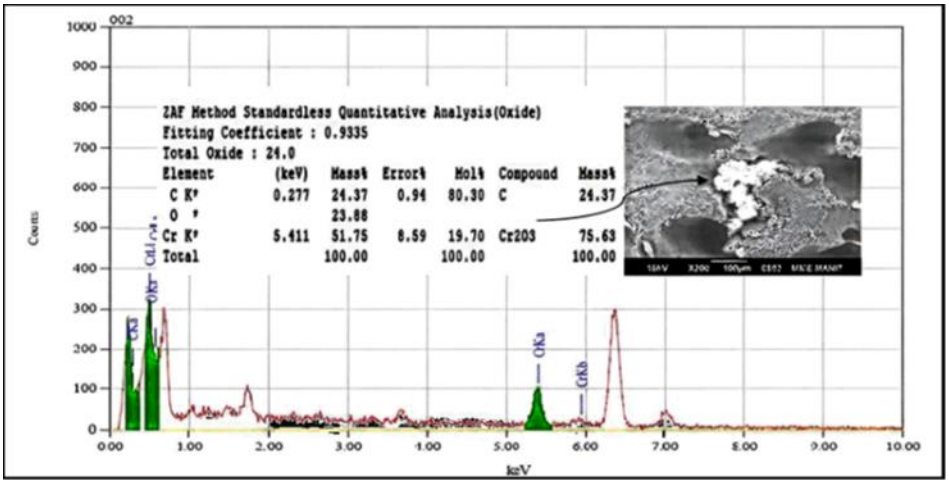
002
ZAF Method Standardless Quantitative Analysis(Oxide)
Fitting Coefficient : 0.9335
Total Oxide : 24.0
Element (keV) Mass% Error% Mol% Compound Mass%
C K* 0.277 24.37 0.94 80.30 C 24.37
O * 23.88
Cr K* 5.411 51.75 8.59 19.70 Cr2O3 75.63
Total 100.00 100.00 100.00
Counts
keV

Fig. 4 (a-f). SEM images on the leading edges show uniformly distributed pores, and they are deeply penetrating, with an average diameter of 100m. (g) EDX data on the phases eroded away from the leading edges indicates carbon, Cr and oxygen peaks.

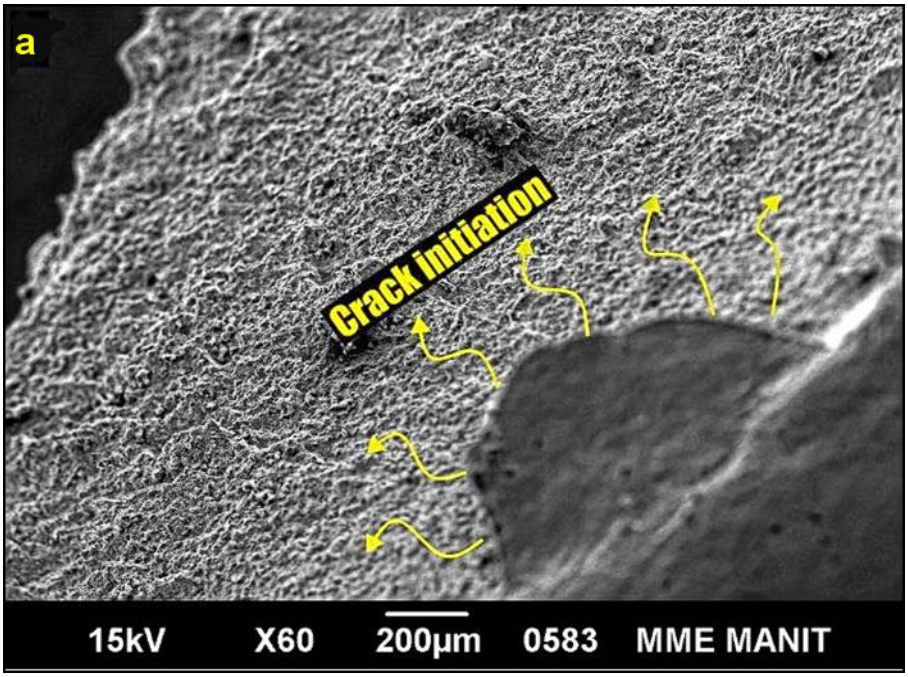

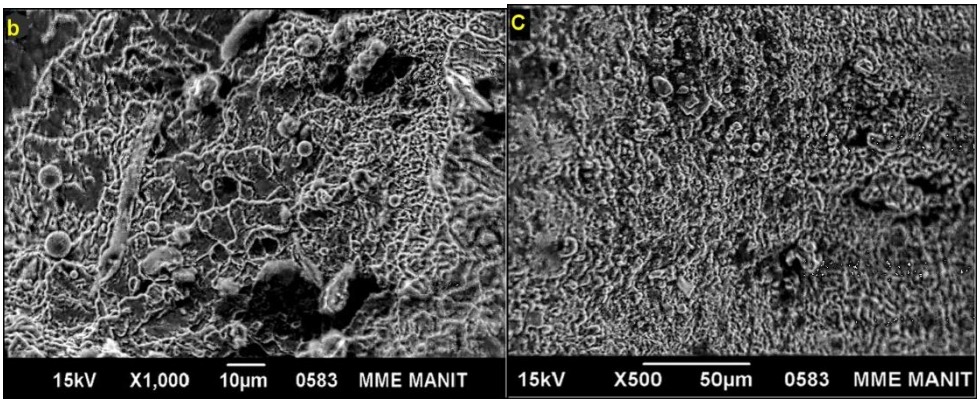

Fig. 5 . (a) Crack originating at the trailing edge of the turbine blade from a shallow pit/pore. Beach marks and ratchet marks are also visible in areas of crack propagation. (b) As the crack propagates, it reveals a smooth surface, indicating an intergranular fracture mode in the zone nearer the crack initiation. (c) Final fast fracture region

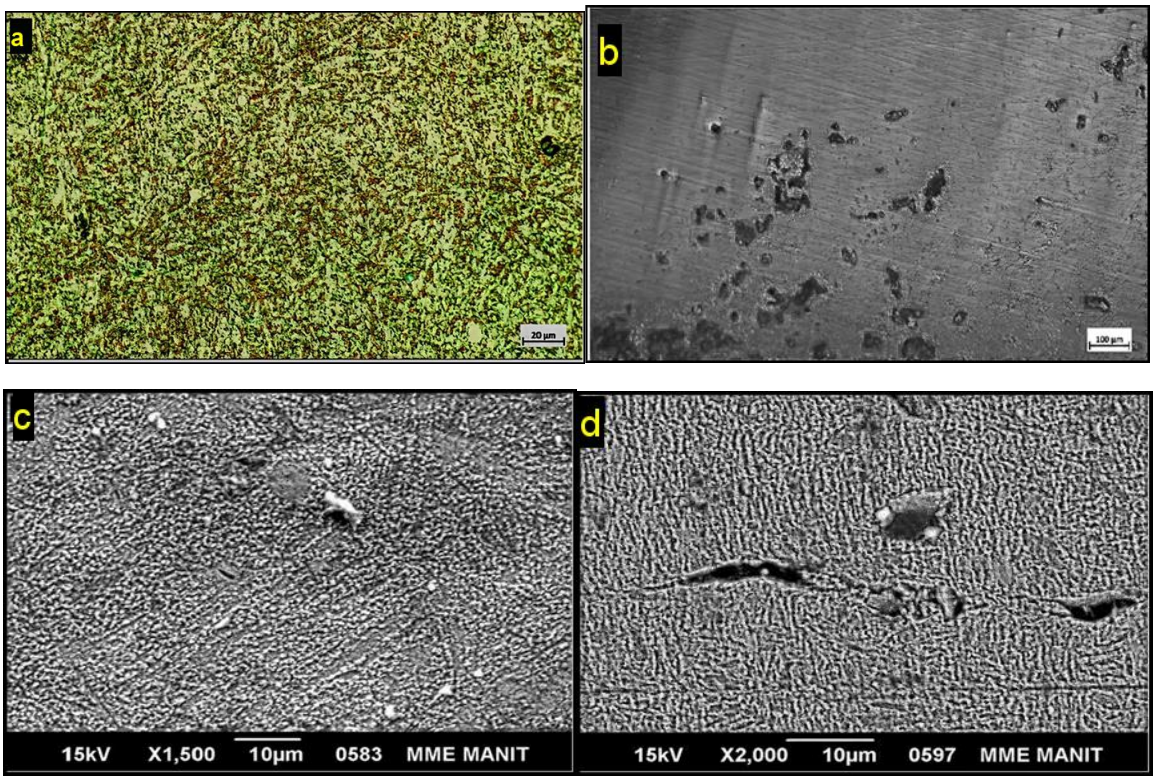
a
20 µm
b
100 µm
c
15kV X1,500 10µm 0583 MME MANIT
d
15kV X2,000 10µm 0597 MME MANIT

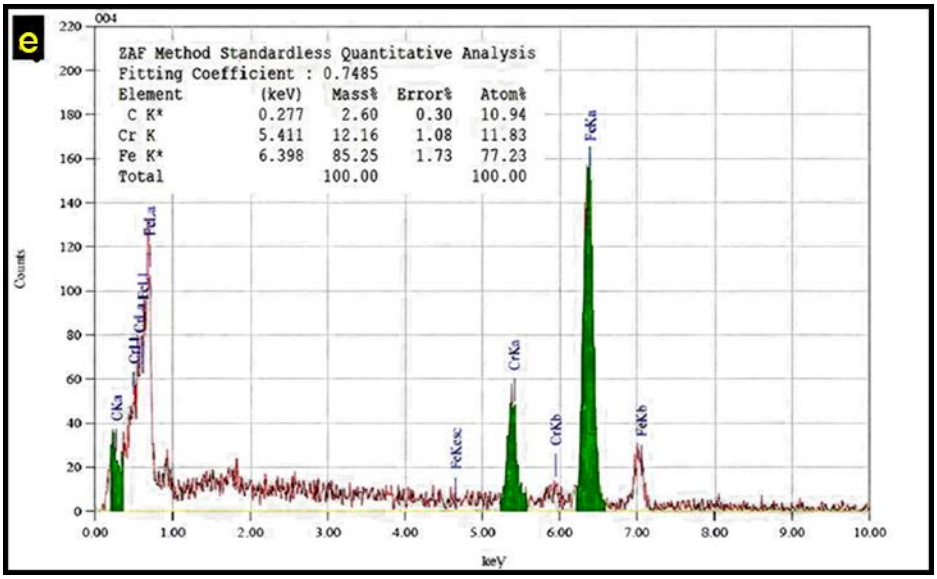
e
004
ZAF Method Standardless Quantitative Analysis
Fitting Coefficient : 0.7485
Element (keV) Mass% Error% Atom%
C K* 0.277 2.60 0.30 10.94
Cr K 5.411 12.16 1.08 11.83
Fe K* 6.398 85.25 1.73 77.23
Total 100.00 100.00
CKa
PdLa
CrKa
FeKesc
CrKb
FeKa
FeKb
Counts
keV

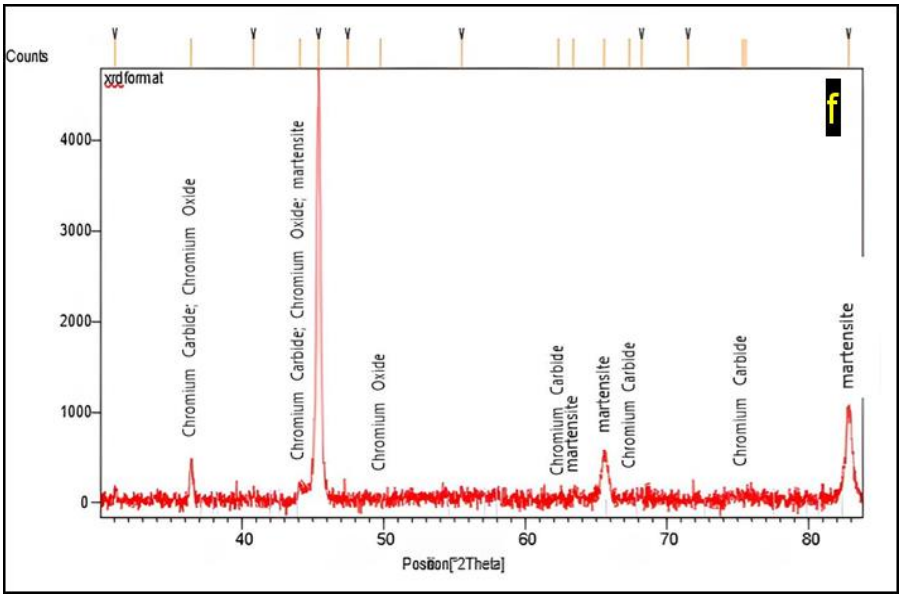

Fig. 6. (a) The optical microscope reveals carbide precipitates on the turbine blade's surface (b) An inclusion rating showed oxide inclusions near the leading edges where pores form (c) SEM microstructure reveals uniform precipitates of chromium carbide within the lath martensitic matrix (d) EDX spectrum on the precipitates (bright spots) indicates chromium and carbon peaks indicating chromium carbide. (e) XRD analysis at the surface near to porous region.

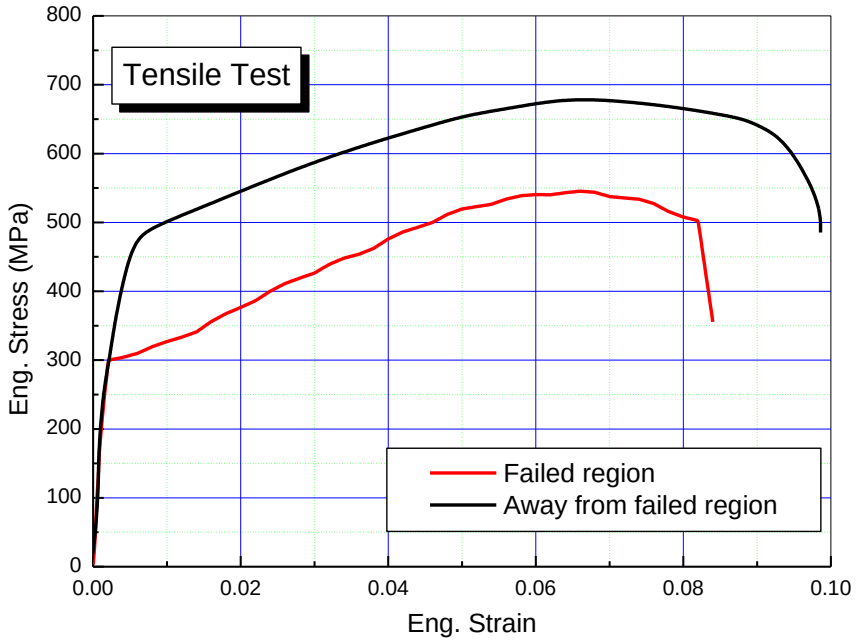

Fig. 7. Tensile test results of the turbine blades in the unfailed region and in the exhust region where it failed.

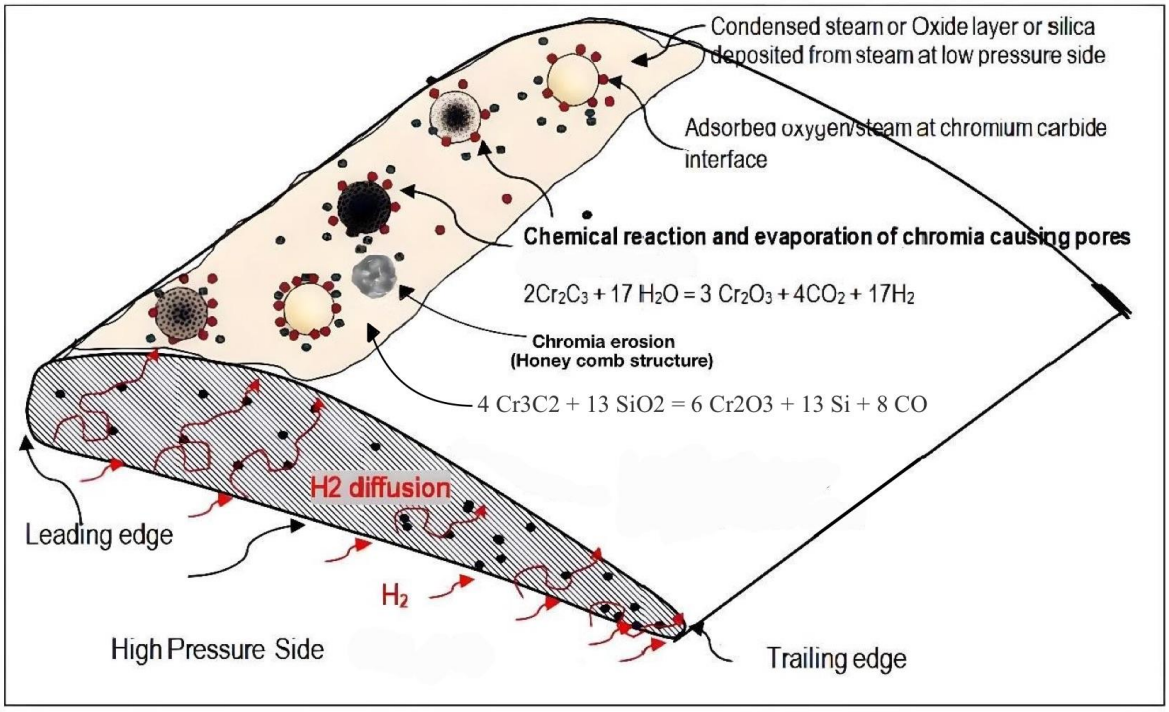

Fig. 8. Visualization of pore formation mechanism in turbine blade under investigation.

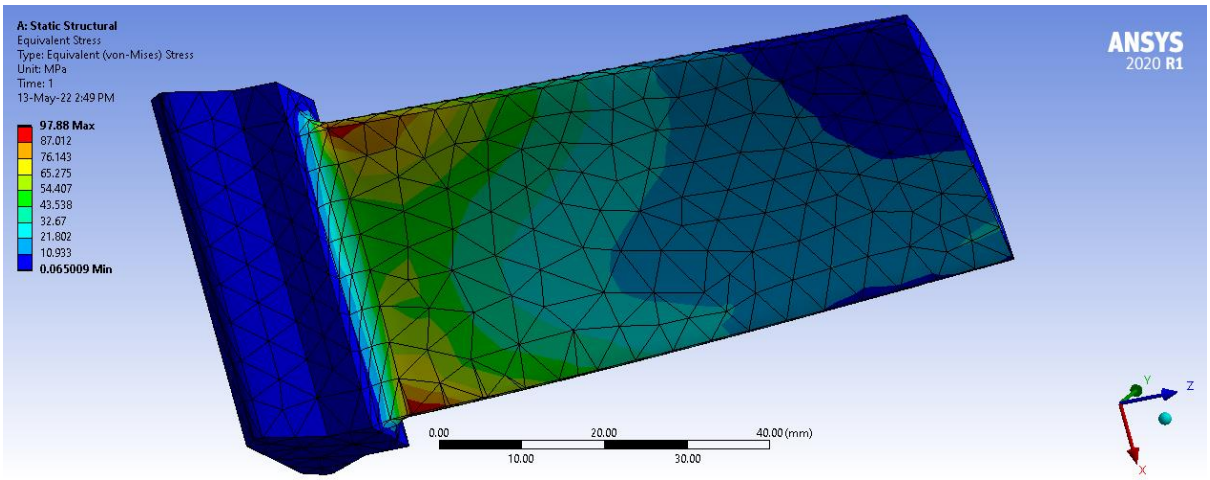

Fig.9. Equivalent Von-Mises stress

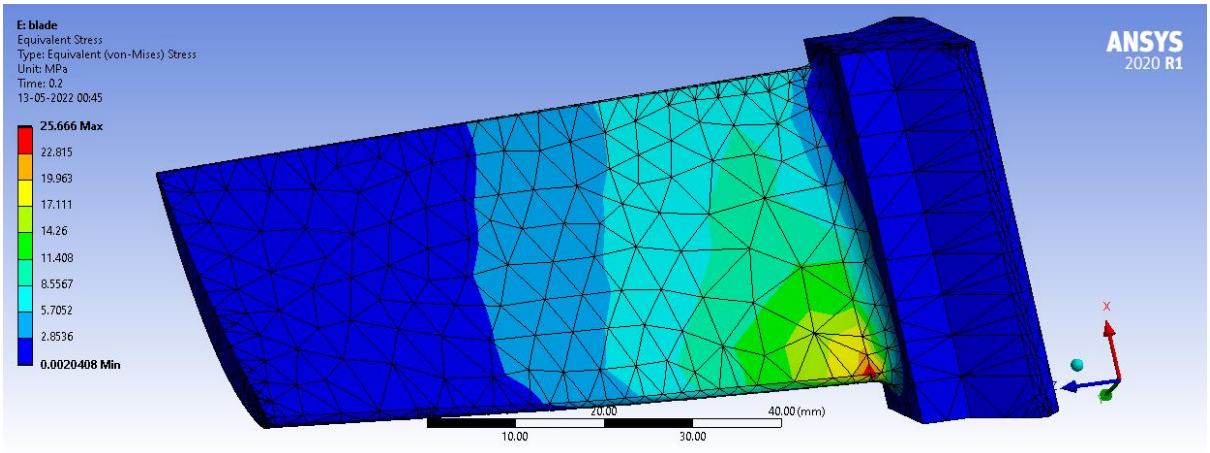

Fig.10. Equivalent Von-Mises stress after pore introduction of 0.1mm

Table 1. The chemical composition of a failed turbine blade

Element	C	Si	Mn	Cr	Ni	S	P	Fe
Wt %	0.18	0.47	0.46	13.84	0.32	0.022	0.021	Bal.

Table 2. Inclusion rating at the region away from the pores and near to the pores.

Inclusions		Away from the pores	Near to the pores
Type A	Sulfides	0	0
Type B	Aluminates	0.5	0.5
Type C	Silicates	0	0
Type D	Globular oxides	1.0 – 1.50	3.0 to 4.0 (Thick)

Table 3. Macro Vickers hardness of failed samples at different locations.

Location	Hardness (HV30)
1	416
2	423
3	432
4	417

Table 4. Micro Vickers hardness of failed samples nearer to the porous region

Location	Hardness (HV0.1)
1	289
2	285
3	285
4	292

Table 5. Showing dryness factor at low, medium and high pressure using Rankine diagram

Temperature(°C)	Sg	Sf	Sfg	x
270	5.4166	2.9765	2.9539	82%
230		2.6193	3.5364	78%
155.3	5.4166	1.8924	4.9002	71.92%

Reply to the comments of Reviewers

The authors are thankful to the reviewers for their valuable comments to improve the quality of paper. The following revisions are made as suggested by reviewers.

Reviewer 1-

1. The changes have improved the paper but I have a concern about the final section prior to the Conclusions when the cycles to failure are calculated.
The estimated critical crack length is 1.252 mm based on KIC but then the author refers to total length of 50 mm in calculating cycles to failure. It is confusing. Please clarify.

The total length is revised as width of specimen which is used for calculating N_f .In the revised manuscript the statements have been revised along with calculations to enhance the clarity (pg 20 , section 4.3.2)

2. Define units of KIC.
Mpa$\sqrt{mm}$, added in revised manuscript

A water droplet erosion-induced fatigue crack propagation and failure in X20Cr13 martensitic stainless-steel turbines working at low pressure

low- pressure turbine Undergoes premature failure

Naked-eye visual inspection

Detailed microscopic and SEM analysis, revealing different details about fracture

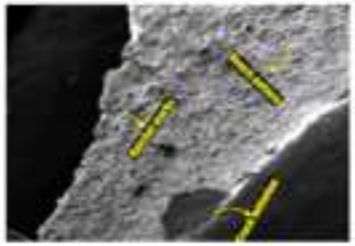

MAGNIFIED VIEW

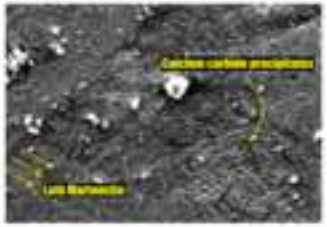

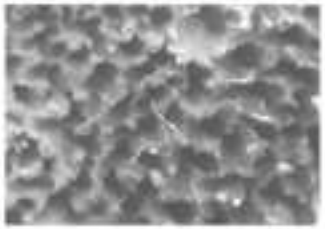

Detailed analysis revealing reasons for fracture

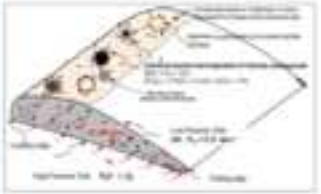

Conclusion

According to the current study, material failures due to defects are entirely eliminated. The failures resulted from the pores created during the operation that concentrated stress, causing cracks to form.

A water droplet erosion-induced fatigue crack propagation and failure in X20Cr13 martensitic stainless-steel turbines working at low pressure

Mohd Sarim Khan[1], C Sasikumar[11♥]
[1]Department of Materials &Metallurgical Engineering, MANIT Bhopal, M.P., India

Abstract

A low-pressure steam turbine blade failed at a thermal power plant reported in this paper. Few blades were damaged on the exhaust side, and the cracks originated on the trailing edge and spread toward the leading edge of blade. In the crack initiation point, shallow corrosion pits were evident, however, turbine vibrations were found to be actuating crack initiation and propagation. Due to numerous pits observed on blades surface, there were vibrations. A pressure drop on the exhaust side of the steam turbine caused condensation and water droplets impinging on the blades caused severe erosion. Upon contact with the condensed water droplets, the chromium carbide precipitates in the martensitic matrix converted into chrome oxides, and impingement of high velocity steam erodes these oxides, causing a rough surface with honeycombed texture. As a result of the roughened blade surfaces, fatigue cracks form at potentially weaker areas and subsequently the final fracture.

Keywords: erosion-fatigue, failure analysis, turbine, x20cr13 martensitic stainless steel, water droplet erosion

[1♥]corresponding author: Dr C Sasikumar, Department of Materials & Metallurgical Engineering, MANIT Bhopal, Madhya Pradesh, India, Email: csasimv@gmail.com, Ph: +91-8989005394

1. Introduction

The failure of a turbine blade in a low-pressure turbine with a capacity of 2500 MW at one of the leading refineries in India is investigated in this study. This turbine is designed to operate at a speed of 6440 rpm, with inlet steam pressure of 17 kg/cm^2, pressure of 10.68 kg/cm^2 inside the turbine, and 0.105 kg/cm^2 at the exhaust side. Steam is generated using a circulating fluidized bed combustion (CFBC) type boiler with petroleum coke as the fuel. The initial steam temperature is 270°C, and steam flows in an axial direction. The temperature at the low pressure side of turbine is about 155^{0}C, which is found to be below the first condensation temperature. Turbine blades attached to the rotor and its design includes a root, shaft, and shroud, with twisted blades on the exhaust side. The moving blades have an inverted T-root with an integral shroud, while the exhaust stage blades are curved with fir-tree roots to reduce the force with which water droplets impact the blade. A lacing wire connects the moving blades of the exhaust stage to reduce vibration. Blades are made of corrosion-resistant martensitic stainless steel X20Cr13 quench hardened and tempered with a tensile strength of 780 MPa, yield strength of 580 MPa and an elongation of 15 percent. The material is designed to sustain more than 10^7 fatigue cycles at 390 MPa in corrosion free environments. Steam quality is maintained through careful control of chlorides, dissolved Fe, Cu, oxygen, silica, etc. to prevent corrosion damage to blades. Few blades at the exhaust side of the turbine broke during its use, and it failed after about 10 years. As shown in figure 1, the fracture appeared about 200-250 mm from its root in the exhaust side blades. The blades failed prematurely, so a root cause analysis was conducted. There were about four shut-downs and start-up attempts in the ten months prior to the final failure.

Several case studies for turbine blade failure are reported earlier as well [1-7]. It has been observed that failure of low-pressure turbine is more frequent and common as compared to

intermediate and high-pressure turbines. Among many some main reasons attributed to failure of steam turbines are improper feed water chemistry, material defects, corrosion by extreme operating conditions, cycle fatigue, concentration of steam contaminations, presence of crevices and turbine vibrations [8-13]. However, blade erosion, combined with turbine vibration, is less well documented as a cause of fatigue crack propagation. The present study addresses these combined effects.

Fig. 1. In the photograph, a fracture is visible about 100 mm from the root of the turbine blade on the exhaust side of the stream turbine.

2. Methodology

We have carried out chemical analysis using a Leco GDS optical spectrophotometer to confirm the material grade, visual examination to identify the fracture origin, fractography using JEOL 6390A SEM (Scanning Electron Microscopy) to identify the mode of failure, metallographic examinations including inclusion rating to find out the micro-constituents responsible for the crack initiation, EDX (Energy Dispersive X-Ray) to find out the micro-chemical analysis of crack originating regions, XRD (X-Ray Diffraction) for identification of phases and whether they have changed over time, Micro Vickers hardness, Rockwell hardness tests to investigate the local and bulk hardness of the blades, an examination of strength and ductility by tensile test and testing the fracture toughness of blade materials using the Charpy impact test.

3. Results

3.1 Visual inspection

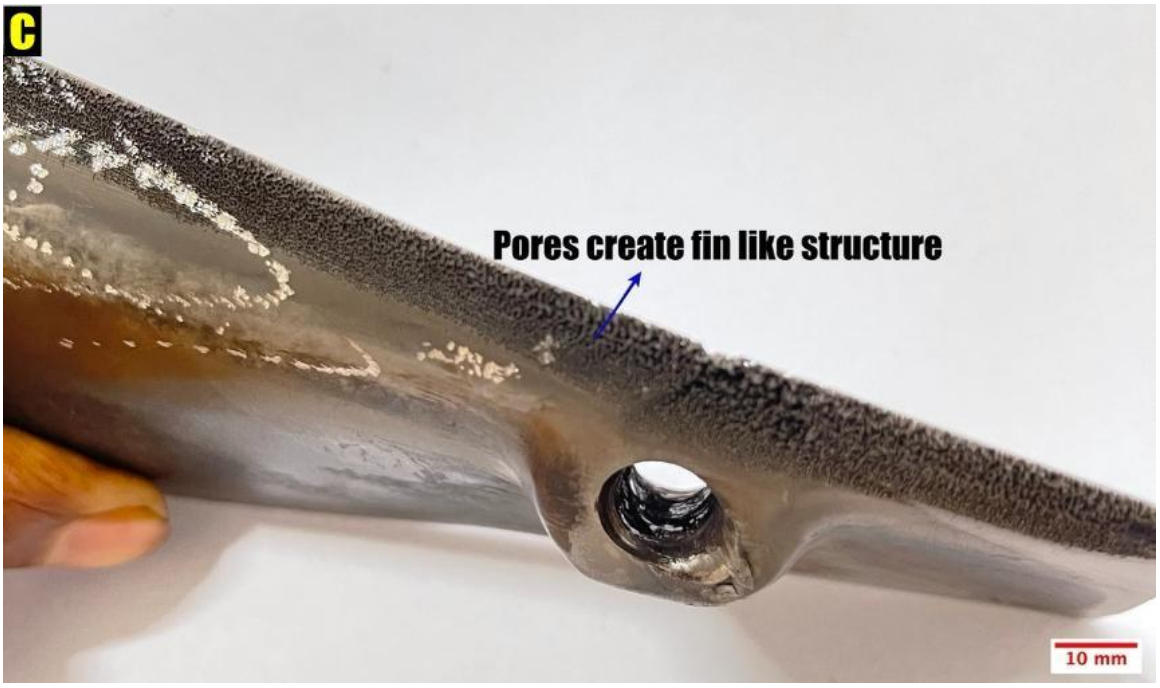

Fig. 2(a, b, c). The leading edges of turbine blades located on the exhaust side show several pits/grooves, an apparent fin-like texture.

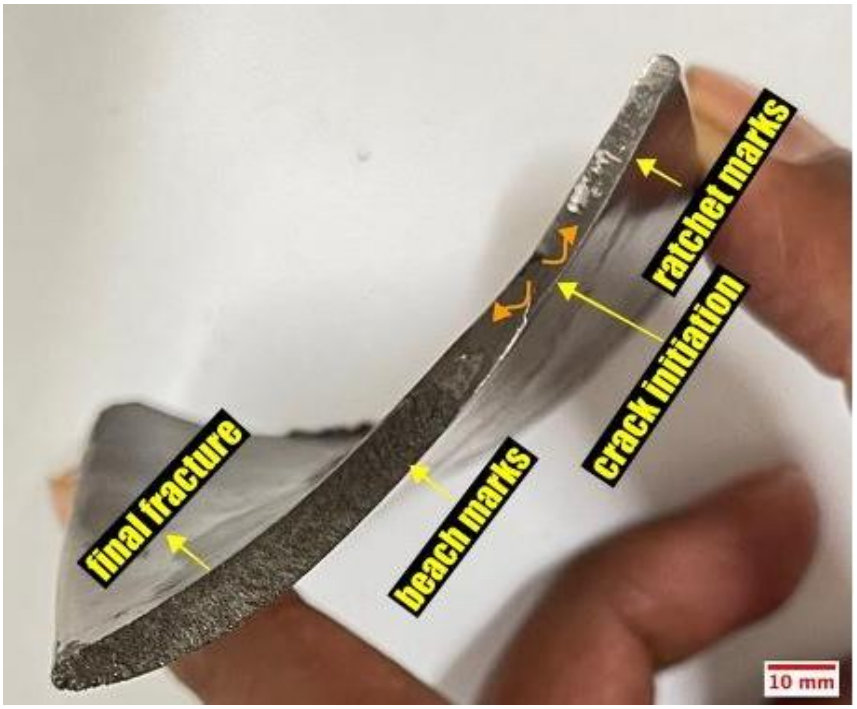

Fig. 3. Fracture surfaces shown in (a) concave and (b) convex perspectives, and (c) cross sections demonstrating crack initiation point, crack propagation region with beach marks and the final fast fracture region.

Turbine blades on the exhaust side of a steam turbine are carefully inspected to discover damage at their surfaces. Figures 2a-c show typical images with fine pores along the leading edge of the blade on the convex side. A close inspection of these surfaces (figure 2c) revealed material was removed at these pores due to erosion/corrosion, resulting in fin-like structures. The fracture surfaces are depicted in Figure 3 a-c at concave and convex sides, as well as in a cross section. The fracture surface (3c) shows brittle and ductile fracture zones as well as beach marks in the crack propagation region that reveal fatigue mode fracture. Beach markings revealed the direction of the cracks and the crack initiation point. In addition, ratchet marks are visible at the fatigue crack regions, suggesting severe stress concentrations there. It is also noted that cracks are originating from different locations and that crack directions change along its path, indicating a torsional load is present at this point.

3.2 Chemical Analysis

The bulk chemical analysis of the turbine blade material is shown in table 1. Using chemical analysis, it was determined that the failed blade was made of the stainless steel AISI 420 grade, which is the same as X20Cr13of European standards. This blade exhibited a negligible amount of molybdenum, which is essential for stainless steel to show pitting resistance. This suggest that the material is having poor pitting resistance.

Table 1. The chemical composition of a failed turbine blade

Element	C	Si	Mn	Cr	Ni	S	P	Fe
Wt %	0.18	0.47	0.46	13.84	0.32	0.022	0.021	Bal.

3.3 Fractography

The low magnification image of the fractured surface of the failed blade at the trailing edge is shown in Figure 4 a-f. There are several pits uniformly distributed on the leading edges, each with a diameter of about 100 millimeters. An examination of these sites close up revealed that bright phases had been eroded away, resulting in the formation of deep pores. EDX analysis of these eroding phases shows Cr, O, and carbon peaks (fig.4g).

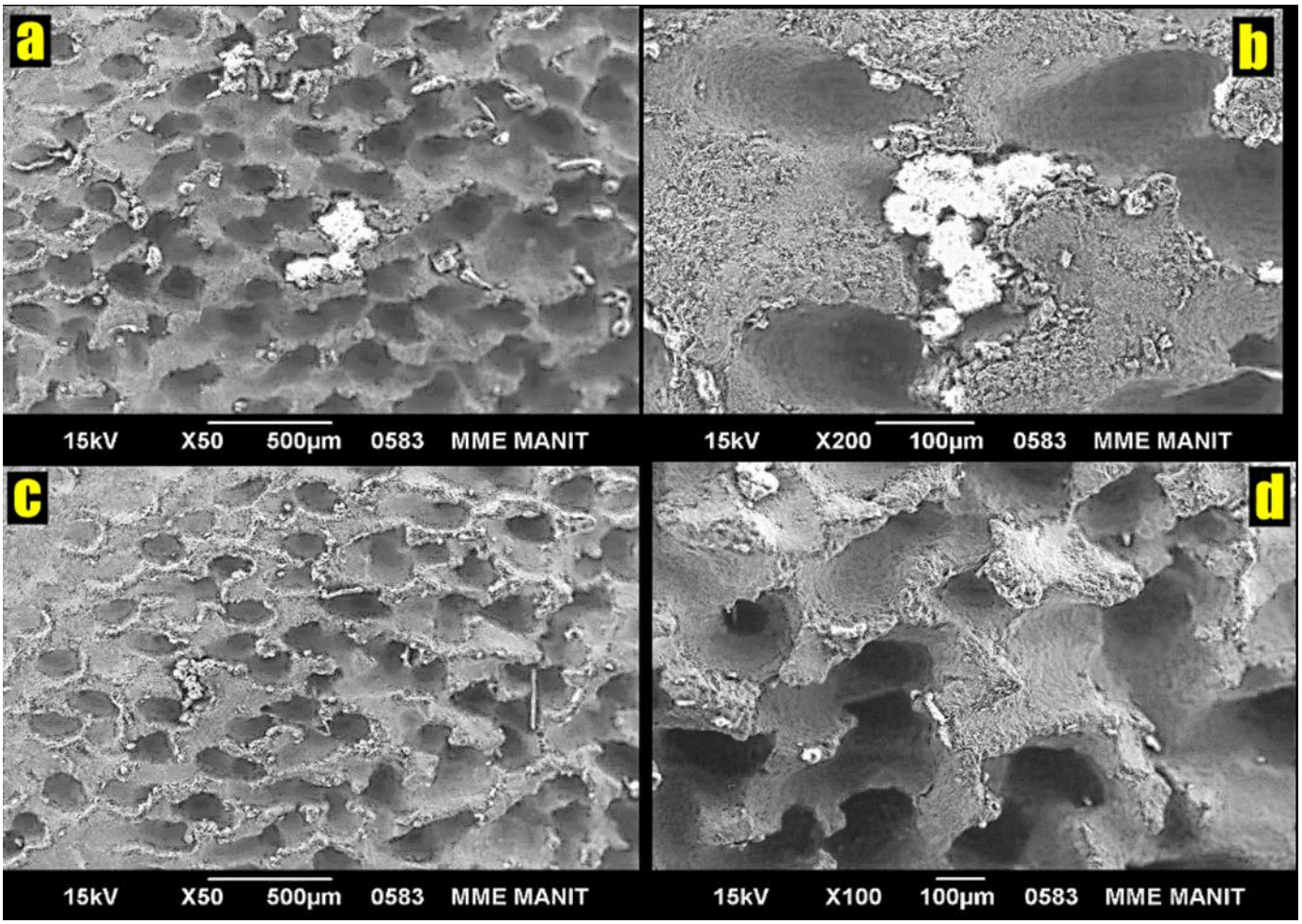
a
15kV X50 500µm 0583 MME MANIT
b
15kV X200 100µm 0583 MME MANIT
c
15kV X50 500µm 0583 MME MANIT
d
15kV X100 100µm 0583 MME MANIT

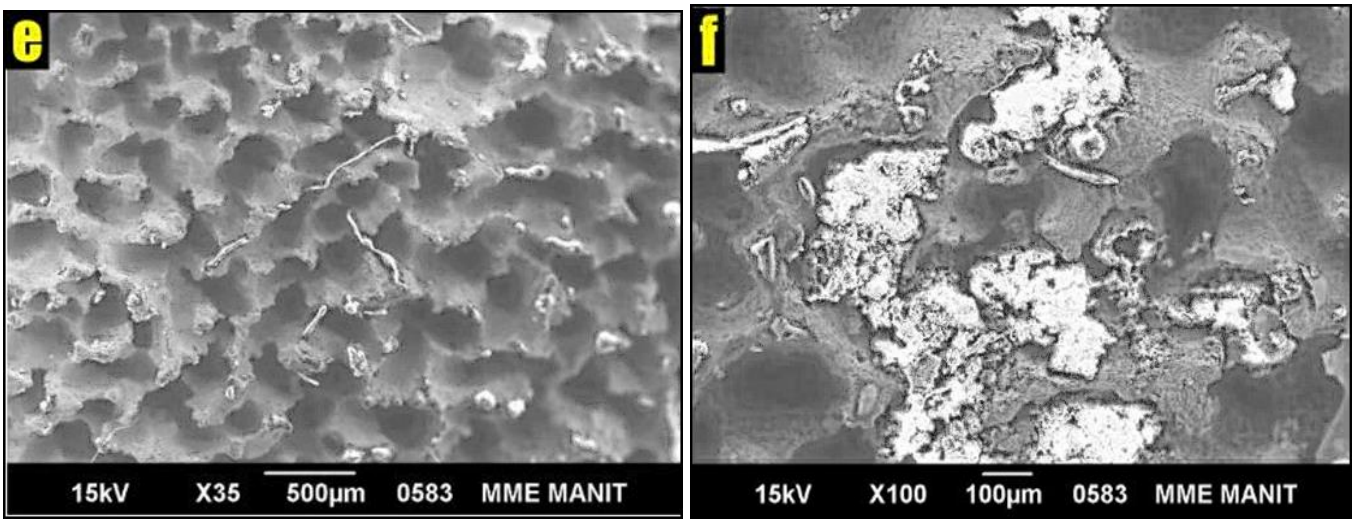
e
15kV X35 500µm 0583 MME MANIT
f
15kV X100 100µm 0583 MME MANIT

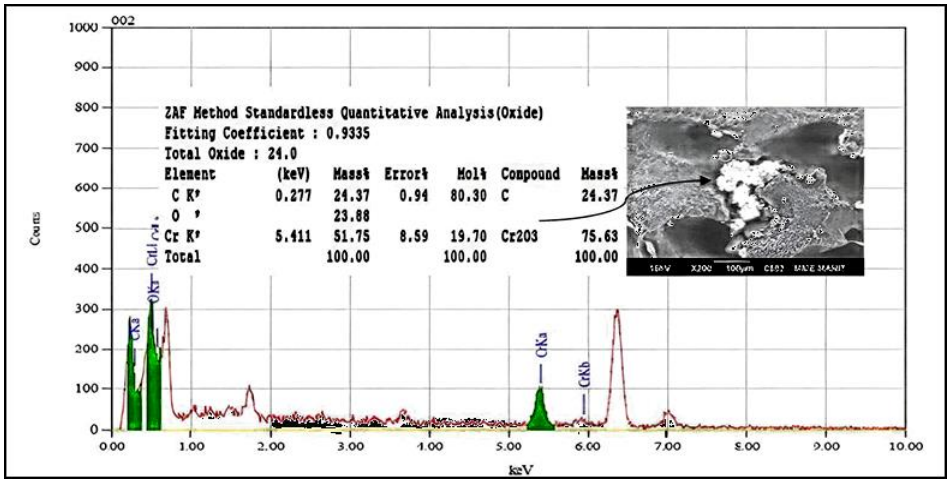
002
ZAF Method Standardless Quantitative Analysis(Oxide)
Fitting Coefficient : 0.9335
Total Oxide : 24.0
Element (keV) Mass% Error% Mol% Compound Mass%
C K? 0.277 24.37 0.94 80.30 C 24.37
O ? 23.88
Cr K? 5.411 51.75 8.59 19.70 Cr2O3 75.63
Total 100.00 100.00 100.00
Counts
keV
CrKa
OKa
CrKb

Fig. 4 (a-f). SEM images on the leading edges show uniformly distributed pores, and they are deeply penetrating, with an average diameter of 100m. (g) EDX data on the phases eroded away from the leading edges indicates carbon, Cr and oxygen peaks.

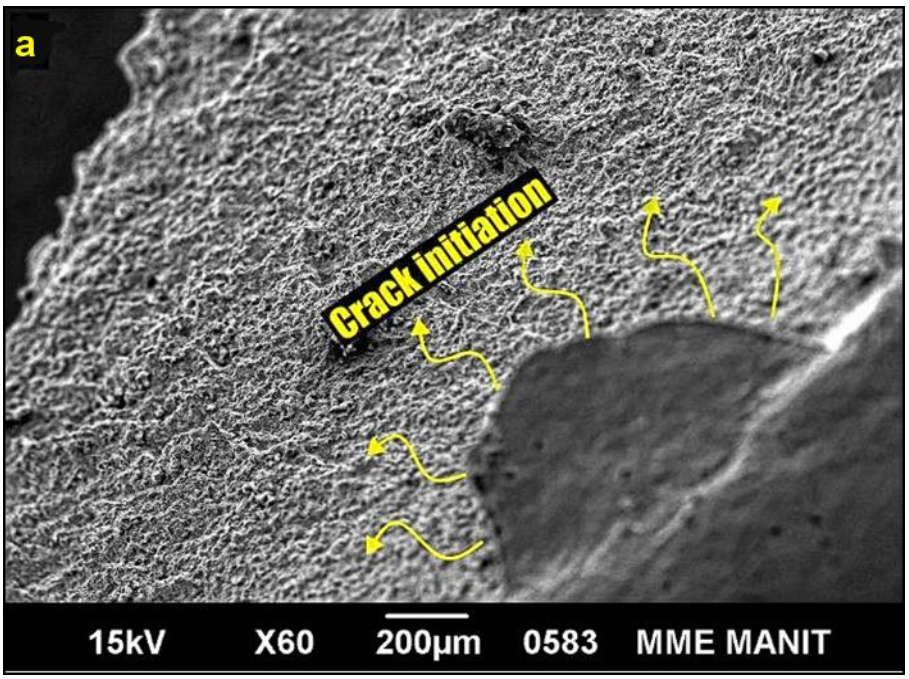

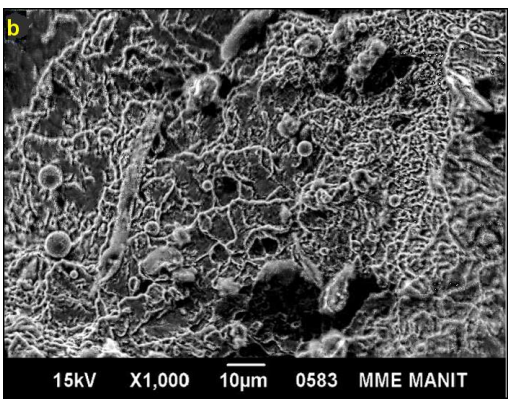

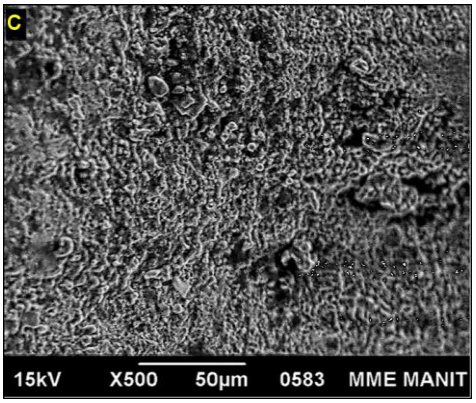

Fig. 5 . (a) Crack originating at the trailing edge of the turbine blade from a shallow pit/pore. Beach marks and ratchet marks are also visible in areas of crack propagation. (b) As the crack propagates, it reveals a smooth surface, indicating an intergranular fracture mode in the zone nearer the crack initiation. (c) Final fast fracture region

In figure 5(a), the crack found originates from the trailing edge of the turbine blade, even though the leading edge has several deep pores. A crack that originates from a shallow pit/pore

located near the trailing edge of the turbine blade. In crack propagation regions, beach marks as well as ratchet marks can be observed. The ratchet marks in different directions indicate how the direction of the crack changes as the turbine blade rotates.

3.4 Microstructural, EDX and XRD Analysis

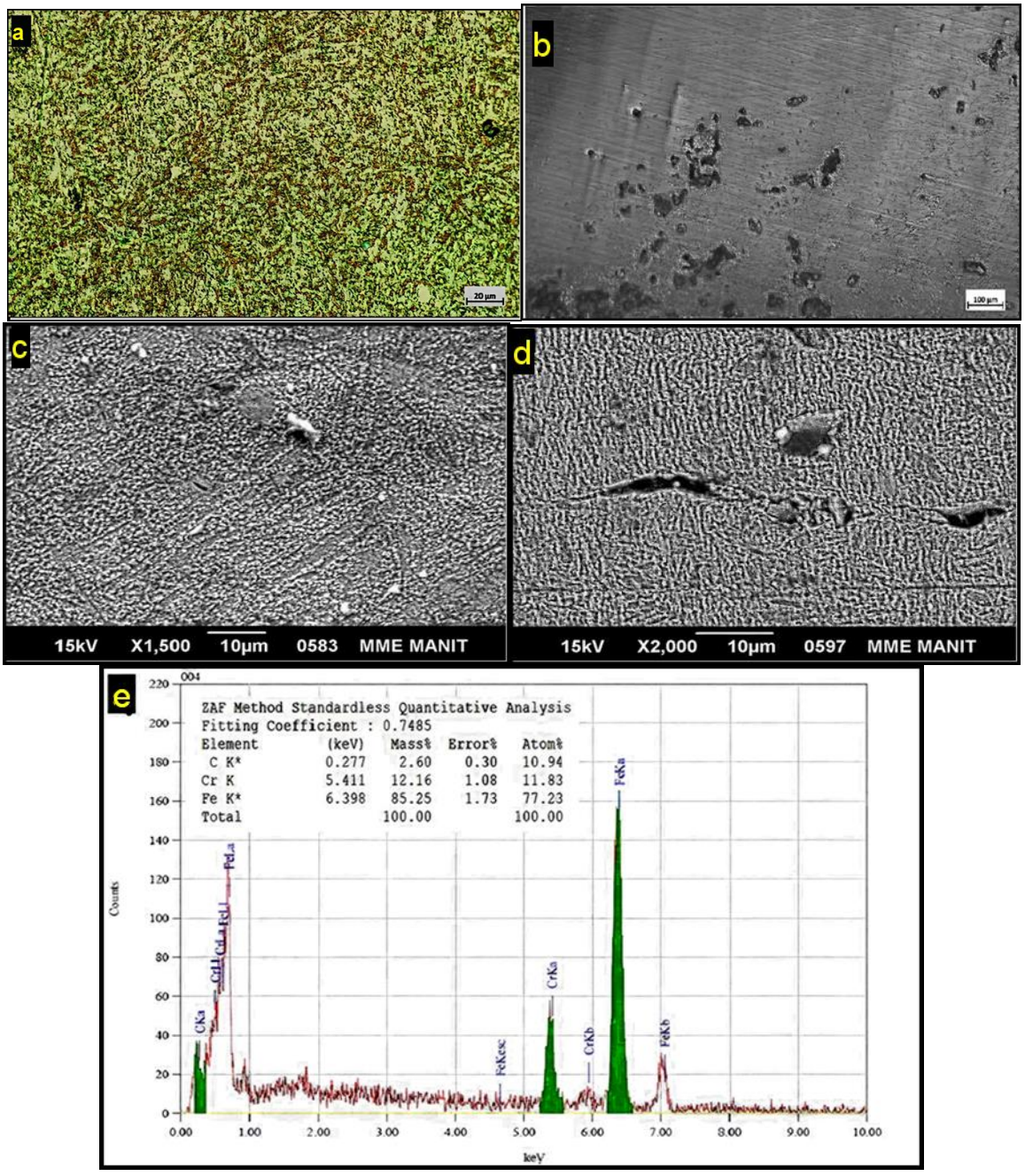

10

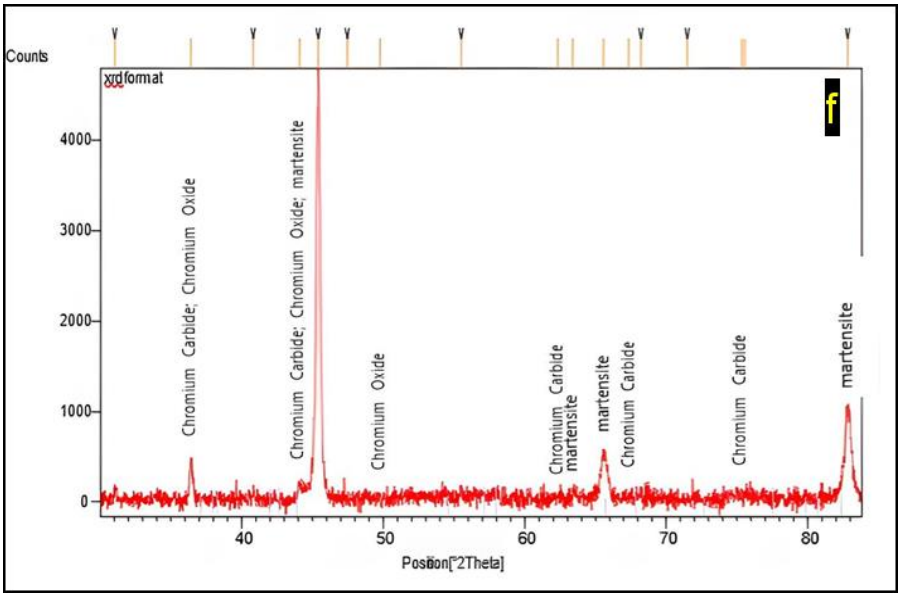

Fig. 6. (a) The optical microscope reveals carbide precipitates on the turbine blade's surface (b) An inclusion rating showed oxide inclusions near the leading edges where pores form (c) SEM microstructure reveals uniform precipitates of chromium carbide within the lath martensitic matrix (d) EDX spectrum on the precipitates (bright spots) indicates chromium and carbon peaks indicating chromium carbide. (e) XRD analysis at the surface near to porous region.

As can be seen in figure 6 a and b, the optical microscopy images show the surface microstructure and inclusions near the porous region of the turbine blade. The surface microstructure revealed uniformly distributed carbides in the matrix phase. The presence of oxide inclusions is significantly increased at the failed region. A rating of the sample's inclusion is performed at different parts of the sample, and the typical results are shown in Table 2.

Table 2. Inclusion rating at the region away from the pores and near to the pores.

Inclusions		Away from the pores	Near to the pores
Type A	Sulfides	0	0
Type B	Aluminates	0.5	0.5

11

Type C	Silicates	0	0
Type D	Globular oxides	1.0 – 1.50	3.0 to 4.0 (Thick)

The SEM microstructure reveals lath martensite and chromium carbide precipitates uniformly distributed within it (fig. 6c). Microcracks can be seen at a few locations on the concave side of the turbine blade (fig. 6d). The EDX spot analysis shows chromium and carbon peaks in addition to iron peaks, indicating that the precipitates are chromium carbide. The xrd results obtained at the region of failed surface is shown in figure 6f. The analysis revealed martensite as a predominant phase in the steel and also confirmed the presence of chromium carbide and chromium oxide.

3.7 Hardness

The hardness of the failed turbine blade is shown in table 3 and the surface hardness of the failed sample nearer the failed region are listed out in table 4 shown below

Table 3. Macro Vickers hardness of failed samples at different locations.

Location	Hardness (HV30)
1	416
2	423
3	432
4	417

Table 4. Micro Vickers hardness of failed samples nearer to the porous region

Location	Hardness (HV0.1)
1	289
2	285
3	285
4	292

On average, the samples have a surface hardness of 422 HV, which is reduced in the porous region.

3.8 Tensile Test Results

The tensile test results of the samples in the failed and unfailed regions are shown in figure 7.

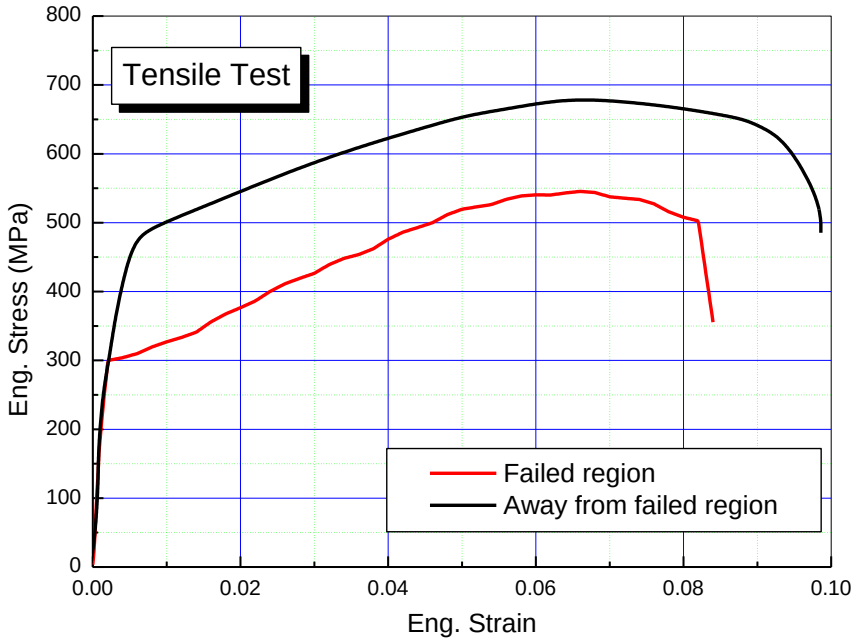

Fig. 7. Tensile test results of the turbine blades in the unfailed region and in the exhust region where it failed.

The tensile test revealed a yield strength of 500 MPa and a tensile strength of 690 MPa in the unfailed region and a yield strength of 310 MPa and a tensile strength of 550 MPa in the

failed region. The ductility also reduced in the failed region. In response to hydrogenating conditions, metallic components are susceptible to hydrogen embrittlement, which results in severe mechanical degradation [14-18]. Hydrogen embrittlement exhibits a prominent loss of strength, ductility, fracture toughness, and fatigue durability as reported elsewhere [19-23],

Furthermore, the samples were also subjected to Charpy impact tests. The Charpy impact values of the un failed samples were about 11 J, while those of the failed samples ranged from 7 to 9 J. In the failed samples, micro indentation tests also revealed cracks that originated after indentation. It is clear from this that the material is susceptible to cracking after being used. The fracture toughness calculated from these local sites using microhardness results are K_{IC} =0.5 to 1.5 MPa.$m^{-1/2}$ nearer to the pores. The reduction in the fracture toughness and ductility could be attributed to hydrogen solubility in the material.

4. Discussions

The following factors were considered to determine the likelihood of steam turbine blade failure: (i) whether the material used for the blades was defective? (ii) Operating conditions affected the degradation and failure of the blade in any way? The chemical composition of the turbine blade material is in accordance with the standards i.e., the turbine is made of X20Cr13 martensitic grade stainless steel. Based on its microstructure, the blade material shows no signs of inhomogeneity or microstructural defects at its original state. The inhomogeneities and degradation observed in the failed sample might have occurred during subsequent operations due to hydrogen adsorption. It has been shown that stainless steels display strong hydrogen-twin interactions, such that the twins act as the medium for rapid hydrogen diffusion, resulting in voids and cleavage at certain locations [24-26]. Based on the inclusion ratings of the sample,

14

the inclusions are prescribed in the original material and Hardness is comparable to that of tempered martensite [1]. Therefore, any possibility of material failure due to material defects is eliminated in the supplied condition. Several grooves were visible on the leading edges of the blade. In a visual inspection these pits appear to be textured like fin-like structures. Close observation of these pits revealed honeycomb morphology and fractographic analysis showed they are about 100 μm in diameter and penetrated deep into the steel. Some of these pores had brightly colored phases, indicating that they may have exuded during the operation. It was found that these are chromium oxides. Chromium oxides were found to have been eroded by steam, leaving a porous region. When we move along the blade's surface, we may notice chromium carbides at the places where chromium oxide is present. Other research studies also reported such erosion marks [2]. It implies that chromium carbide is converted into chromium oxide at these specific locations. Pores are formed when steam impinges on these surfaces, eroding away the chrome oxides. The chemical reactions leading to this pitting corrosion is described below

$2Cr_2C_3 + 17\ H_2O = 3Cr_2O_3 + 4CO_2 + 17H_2$ ……(1)

Other causes of pore formation have also been reported. It is proposed that hydrogen diffuses through the metal and resides at the interfaces of chromium carbides [3,4]. Due to its atomic state, hydrogen in this form is active and forms H_2O after interaction with condensed steam. Oxygen, however, is needed for this reaction to occur. Oxygen may be provided by one or more of the sources listed below. (i) Steam condensing at the low-pressure side because of pressure drop [5]. (ii). Silica deposited by condensation of steam [6]. (iii). A surface oxide scale facilitates the diffusion of oxygen from the atmosphere [7]. Following the formation of steam at the interfaces of chrome carbides, it attacks the carbides and forms chrome oxide, as shown below

$$H_2O_{(g)} \overset{448K}{\longleftrightarrow} H_2O_{(l)} \text{……...…….(2)}$$

$$2Cr_2C_3 + 17\,H_2O \overset{298\ K}{\longleftrightarrow} 3Cr_2O_3 + 4CO_2 + 17H_2$$ ……..(3)

During the evaporation of the chromia from these sites, circular pores appear. Alternately, by silica deposition as a result of pressure drop at the exhaust

$SiO(OH)_2$ (g) in steam + 1/4 O_2 (g) = SiO_2 (deposits) + H_2O (g) ……(4)

4 Cr_3C_2 + 13 SiO_2 = 6 Cr_2O_3 + 13 Si + 8 CO ……(5)

As discussed above, chromium carbides react chemically with steam, resulting in chromia formation and subsequent evaporation at low pressure side of turbine blades [8], creating circular pores. The pore formation mechanism can be visualized in Figure 8.

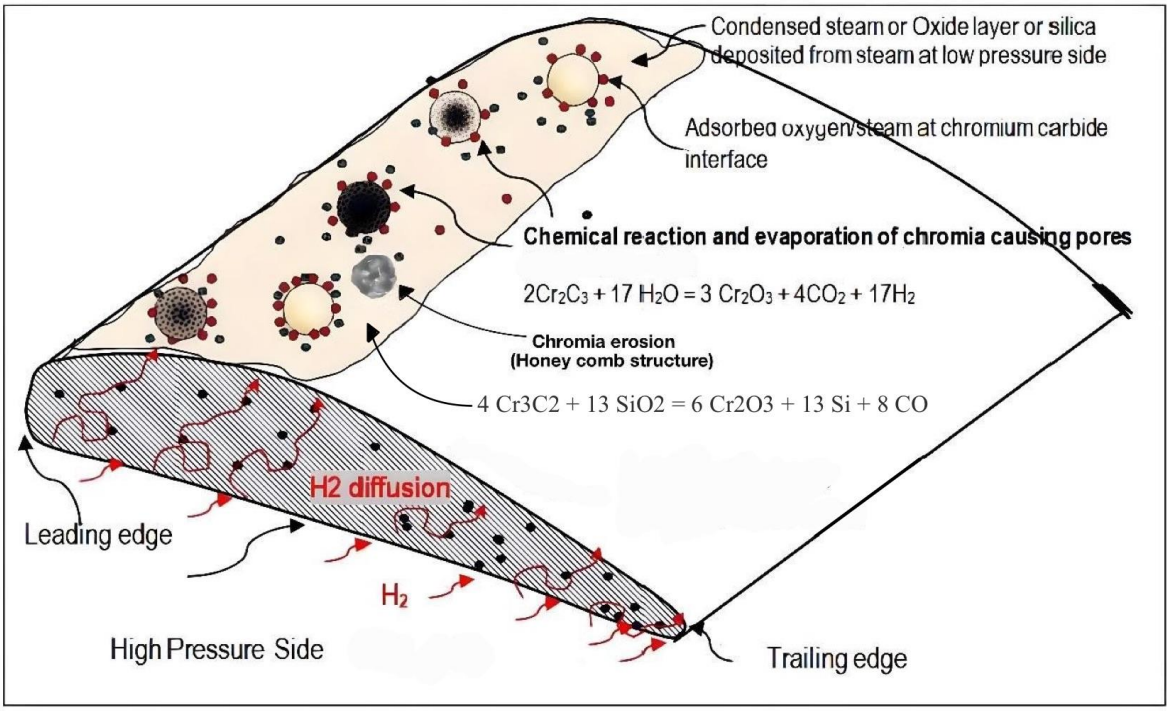

Fig. 8. Visualization of pore formation mechanism in turbine blade under investigation.

4.2 Causes of Pore Formation at Specific Locations

There is a temperature reduction observed a few incidences, to about 230°C, otherwise, HP, MP, and LP steam temperatures are about 333°C, 270°C, and 155°C, respectively. We have calculated the dryness factor (x) at these temperatures corresponding to the high pressure,

medium pressure and low-pressure regions using Rankine diagram and the equation given below

$Sg = Sf + x. Sfg$ ……(6)

The results are given in the table 5.

Table 5. Showing dryness factor at low, medium and high-pressure using Rankine diagram

Temperature(°C)	Sg	Sf	Sfg	x
270	5.4166	2.9765	2.9539	82%
230		2.6193	3.5364	78%
155.3	5.4166	1.8924	4.9002	71.92%

As seen from table 5 the dryness factor at the exhaust is about 72% and the wetness is 28%. Although the value is within the prescribed limit; there is the possibility of steam condensation at exhaust. i.e., The condensation will occur where pressure drop is there [9] i.e., at exhaust region where the percent wetness is increased. Taking steps to reduce this percent wetness may help reduce condensation.

In addition, it is important to note that temperatures and pressures inside turbines fluctuate during operation, especially during start-up and shutdown [10]. Hence, there are locations that will experience cyclic dry/wet steam conditions. Due to local supercooling of the steam flow and the presence of impurities, early condensate could also form above the saturation temperature [6,11]. Surfaces where liquid films are formed have varying thicknesses and continuity depending on steam moisture, chemical impurities, wettability, and rotation speed [12].

4.3 Reasons of Failure of Turbine Blades

According to our analysis, there is an initiation, growth, and ductile regions of failure that confirm that the failure mechanism is high cycle fatigue (HCF). The crack originates on the high-pressure side, even though the pores are on the low-pressure side. This could be attributed to the turbine vibration. Turbine vibration is caused by the formation of pores at the leading edges [13,27,28]. As a result of turbine vibration, fatigue cracks expand from pores and microcracks in the turbine blades. The pores present near to the concave surface (high pressure) have contributed for the crack initiation [28,29]. During rotation at 6440 RPM, the turbine blade will experience the following stress as simulated in Ansys software.

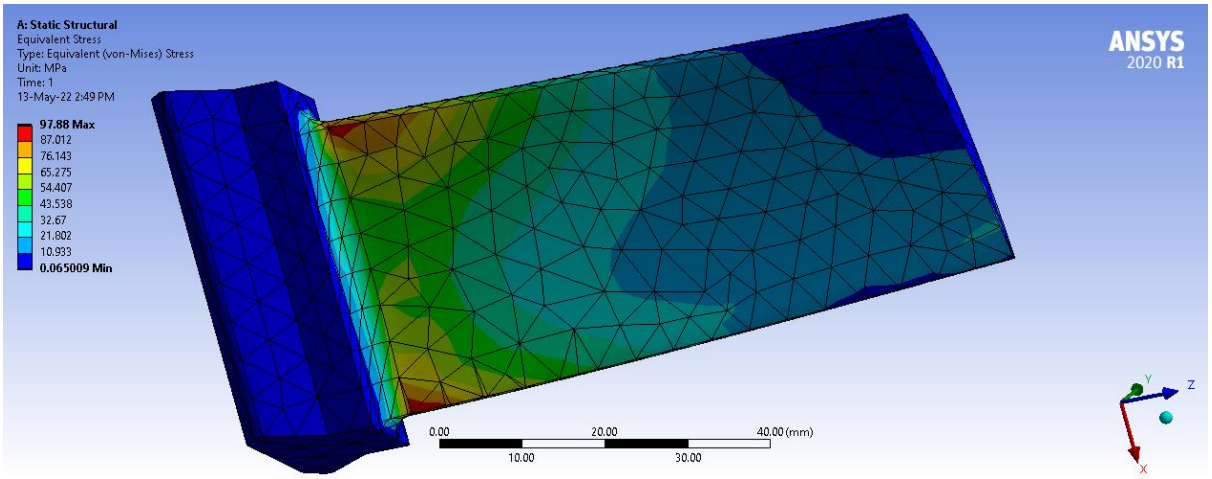

Fig.9. Equivalent Von-Mises stress

Figure 9 shows peak stress 97.88 Mpa, and Avg. stress of 15 Mpa was observed. However, the presence of pores/grooves causes crack initiation [29,30,32.33].

18

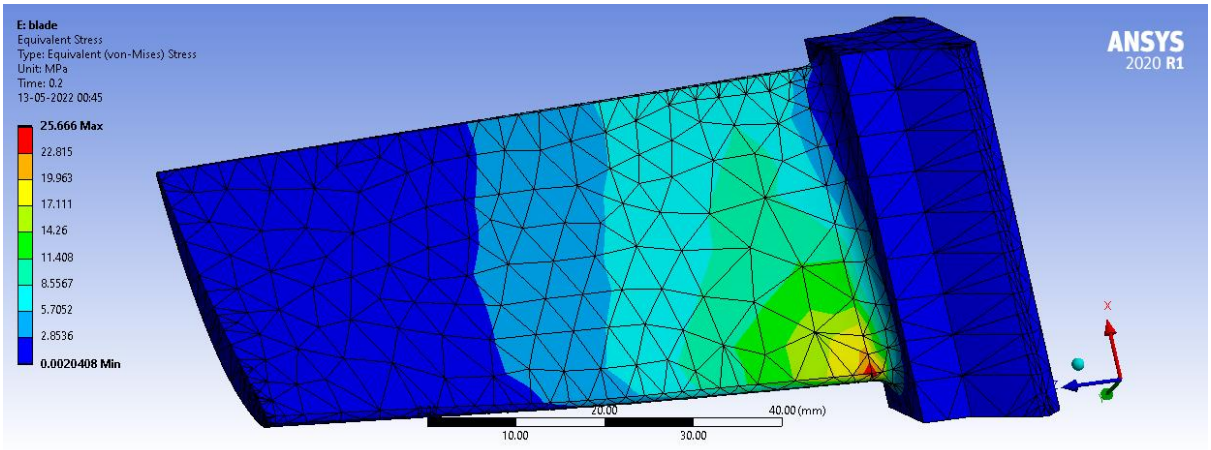

Fig.10. Equivalent Von-Mises stress after pore introduction of 0.1mm

Figure 10 shows that the crack would begin at 25.66 MPa if the material has pore/grooves of 0.1 mm. As the turbine blades are experiencing a stress of about 97.88 MPa, cracks are propagating from the pores on the high-pressure side. Thus, the pores and microcracks at the concave surfaces had made the blades vulnerable for crack initiation and fatigue failure. Few other studies also showed similar reports [30,31,35].

4.3.1 Critical crack length

Here, we have assumed the crack to be a semielliptical notch with radius 0.1 mm and crack length to be 0.5 mm, thus critical crack length is calculated as [36]

$$a_{cr} = \frac{1}{\pi}\left(K_{ic} \Big/ \left\{1.12\sigma_{max} k\left(\frac{a}{b}\right) f_2(\lambda,\delta)\right\}\right)^2 \quad \text{.....(7)}$$

Where,

a_{cr} – critical crack length

K_{1c}- plane strain fracture toughness

σ_{max}- maximum stress

the critical crack length was calculated out to be 1.252 mm with K_{1c}= 250 Mpa$\sqrt{mm}$ for martensitic stainless steels, k(a/b)= 1.15 , and f_2 (λ,δ)= 1.

4.3.2 Unstable crack length and crack propagation life

19

When stress range exceeds a threshold value crack initiated begins to propagate following paris law,[37]

$$\frac{da}{dN} = C(\Delta K)^m \quad \text{.....(8)}$$

Where,

$\frac{da}{dN}$- crack propagation per load cycle

ΔK- stress intensity factor $\Delta K = 1.12\left(\Delta\sigma\sqrt{\pi a}\right)$ .....(9)

Constants C & m are material parameters.

C is 2.02 x 10^{-11} and m is 2.66 for martensitic stainless steels

Thus, crack propagation is 0.291 microns/cycle.

For crack life propagation no. of cycles to failure can be calculated Using Paris-Erdogan equation,

$$N_f = \frac{1}{C(\Delta\sigma)^m\left(\sqrt{\pi}\right)^m}\int_{a_0}^{a_c}\frac{da}{a^{\frac{m}{2}}\left[0.265\left[1-\frac{a}{W}\right]^4+\frac{0.857+0.265\frac{a}{w}}{\left[1-\frac{a}{W}\right]^{\frac{3}{2}}}\right]^m} \quad \text{.....(10)}$$

Where,

a – crack length

a_0 – initial crack length – 0.1 mm

a_c – critical crack length – 1.2525 mm

W – width of specimen – 50 mm

Thus, total cycles estimated for the failure is 715190 cycles. Thus life for 200 Hz : 715190/ 200 = 3576 sec = 59.59 mins [37]

5. Conclusions

1. The chemical analysis revealed that the blade is made of the stainless steel AISI 420 grade, which is the same as X20Cr13 of European standards.

2. Based on its microstructure, the blade material shows no signs of inhomogeneity or micro-structural defects at its original state. It is apparent from the inhomogeneities, and degradation observed in the failed sample that it might have occurred during subsequent operations.
3. According to the inclusion ratings of the sample, the inclusions are as specified in the original material; however, severe oxide inclusions were present at the failing leading edges. These conditions might have been caused by silica deposition or pitting corrosion.
4. The strength and hardness of the turbine blade material are comparable to tempered martensite in supplied condition. Despite this, we find that the tensile strength and ductility of the material are lower at the failed regions. It could be explained by the microcracks lying at the lath- martensite interfaces being opened up during tensile loading.
5. It was found that chromium carbide is converted into chromium oxide at these specific locations. These chromium oxides were eroded by steam, leaving a porous region. According to the research, the pores are about 0.1 mm in diameter and penetrate deeper. In operation, the pores caused turbine vibrations, which triggered fatigue cracks to grow.
6. We calculated that during turbine operation, about 97.88 MPa of load is falling on the blades and that cracks can occur if the blade has a pore of 0.1 mm in diameter.
7. Based on the above-mentioned facts, any possibility of material failure due to material defects is eliminated in the supplied condition. The pores were created during the operation, which caused turbine vibrations, resulting in fatigue cracks from the high-pressure side. As a result, the turbine blade failed.

References

[1] R.A. Grange, C.R. Hribal, L.F. Porter, Hardness of Tempered Martensite in Carbon and Low-Alloy Steels, Metallurgical Transactions A. (1977).

[2] M.R. Khajavi, M.H. Shariat, Failure of first stage gas turbine blades, Engineering Failure Analysis. 11 (2004) 589–597. https://doi.org/10.1016/j.engfailanal.2003.08.010.

[3] Y. Liang, P. Sofronis, Toward a phenomenological description of hydrogen-induced decohesion at particle/matrix interfaces, Journal of the Mechanics and Physics of Solids. 51 (2003) 1509–1531. https://doi.org/10.1016/S0022-5096(03)00052-8.

[4] P. Novak, R. Yuan, B.P. Somerday, P. Sofronis, R.O. Ritchie, A statistical, physical-based, micro-mechanical model of hydrogen-induced intergranular fracture in steel, Journal of the Mechanics and Physics of Solids. 58 (2010) 206–226. https://doi.org/10.1016/j.jmps.2009.10.005.

[5] Y. Wei, Y. Li, J. Lai, Q. Zhao, L. Yang, Q. Lin, X. Wang, Z. Pan, Z. Lin, Analysis on corrosion fatigue cracking mechanism of 17-4PH blade of low-pressure rotor of steam turbine, Engineering Failure Analysis. 118 (2020). https://doi.org/10.1016/j.engfailanal.2020.104925.

[6] S. Zhou, A. Turnbull, Steam turbines Part 1-Operating conditions and impurities in condensates, liquid films and deposits, Corrosion Engineering, Science and Technology. (2003) 97–111. https://doi.org/10.1179/147842203225005654.

[7] R. Rajendran, Gas turbine coatings - An overview, Engineering Failure Analysis. 26 (2012) 355–369. https://doi.org/10.1016/j.engfailanal.2012.07.007.

[8] A. Fry, S. Osgerby, M. Wright, Oxidation of Alloys in Steam Environments-A Review, NPL Report. (2002).

[9] M.A.F. Aliabadi, E. Lakzian, A. Jahangiri, I. Khazaei, Numerical investigation of effects polydispersed droplets on the erosion rate and condensation loss in the wet steam flow in the turbine blade cascade, Applied Thermal Engineering. 164 (2020). https://doi.org/10.1016/j.applthermaleng.2019.114478.

[10] B. Li, A.G. Alleyne, A dynamic model of a vapor compression cycle with shut-down and start-up operations, International Journal of Refrigeration. 33 (2010) 538–552. https://doi.org/10.1016/j.ijrefrig.2009.09.011.

[11] W. Wróblewski, S. Dykas, A. Gardzilewicz, M. Kolovratnik, Numerical and experimental investigations of steam condensation in LP part of a large power turbine, Journal of Fluids Engineering, Transactions of the ASME. 131 (2009) 0413011–04130111. https://doi.org/10.1115/1.3089544.

[12] A. Turnbull, CORROSION-MAY 2008 Current Understanding of Environment-Induced Cracking of Steam Turbine Steels, NACE International. (2007).

[13] S.R.J. Saunders, M. Monteiro, F. Rizzo, The oxidation behaviour of metals and alloys at high temperatures in atmospheres containing water vapour: A review, Progress in Materials Science. 53 (2008) 775–837. https://doi.org/10.1016/j.pmatsci.2007.11.001.

[14] M. Dadfarnia, A. Nagao, S. Wang, M.L. Martin, B.P. Somerday, P. Sofronis, Recent advances on hydrogen embrittlement of structural materials, International Journal of Fracture, 196 (2015), pp. 223-243. https://doi.org/10.1007/s10704-015-0068-4

[15] S. Lynch Recent advances on hydrogen embrittlement of structural materials, International Journal of Fracture, 196 (2015), pp. 223-243. https://doi.org/10.1007/s10704-015-0068-4

[16] M.B. Djukic, G.M. Bakic, V.S. Zeravcic, A. Sedmak, B. Rajicic, Hydrogen embrittlement phenomena and mechanisms . Corrosion Science, 30 (2012), pp. 105-123, https://doi.org/10.1515/corrrev-2012-0502

[17] S. Matsuoka, J. Yamabe, H. Matsunaga, Hydrogen embrittlement of industrial components: prediction, prevention, and models Corrosion Engineering, 72 (2016), pp. 943-961, https://doi.org/10.5006/1958.

[18] T. Michler, C. San Marchi, J. Naumann, S. Weber, M. Martin, Hydrogen environment embrittlement of stable austenitic steels, International Journal of Hydrogen Energy, 37 (2012), pp. 16231-16246, https://doi.org/10.1016/j.ijhydene.2012.08.071.

[19] K.A. Nibur, B.P. Somerday, C.S. Marchi, J.W. Foulk, M. Dadfarnia, P. Sofronis, The relationship between crack-tip strain and subcritical cracking thresholds for steels in high-pressure hydrogen gas, Metall. Mater. Trans. A., 44 (2013), pp. 248-269, https://doi.org/10.1007/s11661-012-1400-5.

[20] Y. Ogawa, H. Matsunaga, J. Yamabe, M. Yoshikawa, S. Matsuoka, Unified evaluation of hydrogen-induced crack growth in fatigue tests and fracture toughness tests of a carbon steel, International journal of Fatigue, 103 (2017), pp. 223-233, https://doi.org/10.1016/j.ijfatigue.2017.06.006.

[21] Y. Ogawa, H. Matsunaga, J. Yamabe, M. Yoshikawa, S. Matsuoka, Fatigue limit of carbon and Cr Mo steels as a small fatigue crack threshold in high-pressure hydrogen gas, International Journal of Hydrogen Energy, 43 (2018), pp. 20133-20142, https://doi.org/10.1016/j.ijhydene.2018.09.026.

[22] D. Birenis, Y. Ogawa, H. Matsunaga, O. Takakuwa, J. Yamabe, Ø. Prytz, A. Thøgersen, Interpretation of hydrogen-assisted fatigue crack propagation in BCC iron based on dislocation structure evolution around the crack wake, Acta Materialia, 156 (2018), pp. 245-253, https://doi.org/10.1016/j.actamat.2018.06.041

[23] D. Wan, Y. Deng, J.I.H. Meling, A. Alvaro, A. Barnoush, Hydrogen-enhanced fatigue crack growth in a single-edge notched tensile specimen under in-situ hydrogen charging inside an environmental scanning electron microscope, Acta Materlia, 170 (2019), pp. 87-99, https://doi.org/10.1016/j.actamat.2019.03.032.

[24] Ming K., Li L., Li Z., Bi X., Wang J., Grain boundary decohesion by nanoclustering Ni and Cr separately in CrMnFeCoNi, high-entropy alloys, 5, 0639 (2019).

[25] Seita M., Hanson J. P., Gradečak S., Demkowjcz M. J., The dual role of coherent twin boundaries in hydrogen embrittlement. Nature Communications, 6, 6164 (2015).

[26] Neeraj T., Srinivasan R., Li J., Hydrogen embrittlement of ferritic steels: Observations on deformation microstructure, nanoscale dimples and failure by nanovoiding. Acta Materialia, 60, 5160–5171 (2012).

[27] J.P. Sippel, E. Kerscher, Properties of the fine granular area and postulated models for its formation during very high cycle fatigue—a review, Applied Sciences (Switzerland). 10 (2020) 1–27. https://doi.org/10.3390/app10238475.

[28] M. Ananda Rao, M. v. Pavan Kumar, T.S.N. Sankara Narayanan, S. Subba Rao, N. Narasaiah, Failure Analysis of a Low-Pressure Turbine Blade in a Coal-Based Thermal Power Plant, Journal of Failure Analysis and Prevention. 15 (2015) 750–757. https://doi.org/10.1007/s11668-015-0013-x.

[29] K.H. Mayer, K. Maile, C. Gerdes, Characterisation and quantification of defects in rotors and casings of steam turbines, Materials at High Temperatures. 15 (1998) 249–258. https://doi.org/10.1080/09603409.1998.11689608.

[30] E.M. Mueller, L. Carney, S.T. Ngin, J.L. Yadon, Failure analysis of weld-repaired B-1900 turbine blade shrouds, in: Proceedings of the International Symposium on Superalloys, Minerals, Metals and Materials Society. (2008) 469–477. https://doi.org/10.7449/2008/superalloys_2008_469_477.

[31] D. Janicki, Disk laser welding of armor steel, Archives of Metallurgy and Materials. 59 (2014) 1641–1646. https://doi.org/10.2478/amm-2014-0279.

[32] X. Li, J. Zhang, Q. Fu, E. Akiyama, X. Song, S. Shen, Q. Li, Hydrogen embrittlement of high strength steam turbine last stage blade steels: Comparison between PH17-4 steel and PH13-8Mo steel, Materials Science and Engineering A. 742 (2019) 353–363. https://doi.org/10.1016/j.msea.2018.10.086.

[33] E. Stefan, B. Talic, Y. Larring, A. Gruber, T.A. Peters, Materials challenges in hydrogen-fuelled gas turbines, International Materials Reviews. (2021). https://doi.org/10.1080/09506608.2021.1981706.

[34] C.J. Mcmahon, Hydrogen-induced intergranular fracture of steels, Engineering fracture mechanics 68 (2001) 773-788. www.elsevier.com/locate/engfracmech.

[35] Rzadkowski R., Drewczyński M., Rao J.S, Ranjith M.C., Piechowski L., Szczepanik R., Crack Initiation and Propagation of Compressor Blade of Aircraft Engine, Journal of Vibration Engineering and Technologies, 2(4),371-384,(2014).

[36] Rao J.S. Turbine Blade Life Estimation, Narosa (2000).

[37] Rzadkowski R., Drewczyński M., Rao J.S, Ranjith M.C., Piechowski L., Szczepanik R., Crack Initiation and Propagation of Compressor Blade of Aircraft Engine, Journal of Vibration Engineering and Technologies, 2(4),371-384, (2014).

26